PSF engineering in multifocus microscopy for increased depth volumetric imaging

Bassam Hajj, Mohamed El Beheiry, Maxime Dahan

Biomedical Optics EXPRESS

PSF engineering in multifocus microscopy for increased depth volumetric imaging

Bassam Hajj,[1,2,3,4] Mohamed El Beheiry,[1,2,3] and Maxime Dahan[1,2,3,5]

[1]*Laboratoire Physico-Chimie, Institut Curie, PSL Research University, CNRS UMR168, 75005, Paris, France*
[2]*Sorbonne Universités, UPMC Univ Paris 06, 75005, Paris, France*
[3]*Transcription Imaging Consortium, Janelia Research Campus, 19700 Helix Drive, Ashburn VA, 20147, USA*
[4]*bassam.hajj@curie.fr*
[5]*maxime.dahan@curie.fr*

Abstract: Imaging and localizing single molecules with high accuracy in a 3D volume is a challenging task. Here we combine multifocal microscopy, a recently developed volumetric imaging technique, with point spread function engineering to achieve an increased depth for single molecule imaging. Applications in 3D single molecule localization-based super-resolution imaging is shown over an axial depth of 4 μm as well as for the tracking of diffusing beads in a fluid environment over 8 μm.

OCIS codes: (170.6900) Three-dimensional microscopy; (100.6890) Three dimensional image processing; (100.6640) Super-resolution.

References and links

1. B. Huang, H. Babcock, and X. Zhuang, "Breaking the diffraction barrier: super-resolution imaging of cells," Cell **143**(7), 1047–1058 (2010).
2. C. G. Galbraith and J. A. Galbraith, "Super-resolution microscopy at a glance," J. Cell Sci. **124**(10), 1607–1611 (2011).
3. S. Abrahamsson, J. Chen, B. Hajj, S. Stallinga, A. Y. Katsov, J. Wisniewski, G. Mizuguchi, P. Soule, F. Mueller, C. Dugast Darzacq, X. Darzacq, C. Wu, C. I. Bargmann, D. A. Agard, M. Dahan, and M. G. Gustafsson, "Fast multicolor 3D imaging using aberration-corrected multifocus microscopy," Nat. Methods **10**(1), 60–63 (2012).
4. B. Hajj, J. Wisniewski, M. El Beheiry, J. Chen, A. Revyakin, C. Wu, and M. Dahan, "Whole-cell, multicolor superresolution imaging using volumetric multifocus microscopy," Proc. Natl. Acad. Sci. U.S.A. **111**(49), 17480–17485 (2014).
5. B. Hajj, M. El Beheiry, I. Izeddin, X. Darzacq, and M. Dahan, "Accessing the third dimension in localization-based super-resolution microscopy," Phys. Chem. Chem. Phys. **16**(31), 16340–16348 (2014).
6. B. Huang, W. Wang, M. Bates, and X. Zhuang, "Three-dimensional super-resolution imaging by stochastic optical reconstruction microscopy," Science **319**(5864), 810–813 (2008).
7. I. Izeddin, M. El Beheiry, J. Andilla, D. Ciepielewski, X. Darzacq, and M. Dahan, "PSF shaping using adaptive optics for three-dimensional single-molecule super-resolution imaging and tracking," Opt. Express **20**(5), 4957–4967 (2012).
8. A. Sergé, N. Bertaux, H. Rigneault, and D. Marguet, "Dynamic multiple-target tracing to probe spatiotemporal cartography of cell membranes," Nat. Methods **5**(8), 687–694 (2008).
9. N. S. Cheng, "Formula for the viscosity of a glycerol-water mixture," Ind. Eng. Chem. Res. **47**(9), 3285–3288 (2008).
10. J. N. Mait, "Understanding diffractive optic design in the scalar domain," J. Opt. Soc. Am. A **12**(10), 2145–2158 (1995).
11. S. Jia, J. C. Vaughan, and X. W. Zhuang, "Isotropic three-dimensional super-resolution imaging with a self-bending point spread function," Nat. Photonics **8**(4), 302–306 (2014).
12. S. R. P. Pavani, M. A. Thompson, J. S. Biteen, S. J. Lord, N. Liu, R. J. Twieg, R. Piestun, and W. E. Moerner, "Three-dimensional, single-molecule fluorescence imaging beyond the diffraction limit by using a double-helix point spread function," Proc. Natl. Acad. Sci. U.S.A. **106**(9), 2995–2999 (2009).

1. Introduction

Fluorescence microscopy provides tremendous insight into cellular processes and functions. When high spatial resolution is required, overcoming the diffraction limit in all three dimensions (3D) becomes an important task. Imaging and localizing single molecules is an effective means to this end, and moreover provides sensitive spatial and temporal information

#256814 Received 8 Jan 2016; revised 27 Jan 2016; accepted 27 Jan 2016; published 2 Feb 2016

on biological processes in living matter [1, 2]. When imaging sparse molecules, their centers of emission can be localized to a precision better than the diffraction limit. Commonly, these studies are made in thin samples within the depth of focus of microscope objectives (roughly 700–800 nm). In many biological systems, however, faithful accounts of large 3D extents of a cell must be attained. From a general standpoint, sequential scanning can be used to capture 3D organization and dynamics inside living cells. However, this modality is often too slow or insensitive to record individual fast-moving molecules. Thus, there is a need for ultrasensitive and rapid imaging methods.

Recently we have shown that multifocal imaging using diffractive element enables fast parallel imaging of single molecules in 3D [3] as well as volumetric super-resolution imaging over a depth range of 3.6 µm [4, 5], comparable to the size of important organelles such as the cell nucleus or mitochondria. In this configuration, the effective imaging depth is determined by the axial sampling of each single-molecule emission. Molecules must appear on several planes to be accurately localized via 3D Gaussian fitting. As such, emitters sampled only once (e.g. near the extrema of the detection volume) are usually discarded. To fully benefit from the imaging extent of the multifocus microscope, we combine the multifocus microscopy approach with previously described point spread function (PSF) engineering methods such as astigmatic imaging [6, 7]. In this fashion, single molecules can be localized over 5 µm depth and bright single nanoparticles can be tracked over 8 µm range with high efficiency.

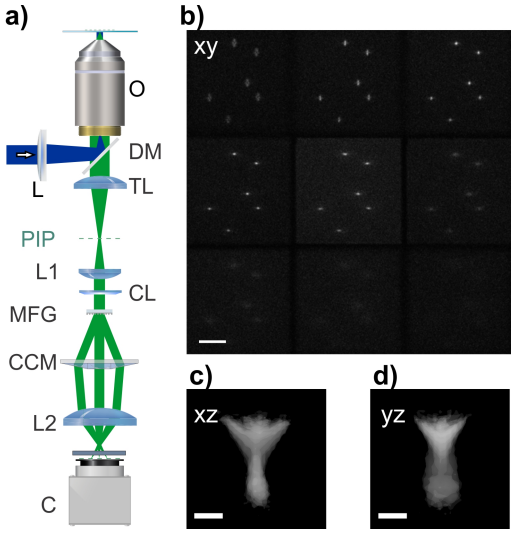

Fig. 1. a) The optical configuration to induce an astigmatic PSF in the multifocus microscope. L: laser, O: microscope objective, DM: dichroic mirror, TL: tube lens, PIP: primary image plane, L1, L2: lens, CL: cylindrical lens, MFG: multifocal grating, CCM: chromatic correction grating, C: camera. b) a snap shot of beads fluorescence as recorded in this optical configuration (scale bar 5 µm). The distorted PSF has an elliptical shape that depends on its axial position compared to each subpanel of the image. c) and d) xz and yz rendering of the distorted PSF showing the induced astigmatism. Scale bar 1 µm.

2. Setup

Our setup is based on the reported multi-focus microscope (MFM) scheme illustrated Fig. 1(a). A diffraction grating (multifocal grating: MFG) is introduced in the emission pathway of a widefield microscope in a plane conjugated to the back focal plane of the imaging objective. The grating motif is optimized to split the emitted wavefront into nine equal intensity diffraction orders. Additional spatial chirp distortion in the grating induces a diffraction order-dependent phase shift in transmitted wavefronts. As such, order-specific defocusing is applied to the different diffracted wavefronts. Nine images are then formed simultaneously on

#256814 Received 8 Jan 2016; revised 27 Jan 2016; accepted 27 Jan 2016; published 2 Feb 2016

different areas of the detector (CCD camera), corresponding to nine axial sections on the sample spaced by a given dz.

For additional PSF engineering, we placed a cylindrical lens (CL) of very long focal length (f = 10m) in the infinity space of the setup, e.g. between the objective and the tube lens or its conjugated space near the grating. The wavefront profile emanating from molecules within the volume is then influenced not only by the defocusing function introduced by the grating but also with the astigmatism induced by the cylindrical lens (Fig. 1(b)). The PSF has thus an elliptical shape (Fig. 1(c), 1(d)), where the ratio of the sizes of the long and short axes encodes for the axial position of the emitter along the optical axis. In such a configuration, sampling on multiple focal planes is not necessary to localize the z position of single emitters. Figure 1(b) shows a snap shot of the beads in a fixed axial position. When in focus in a given panel, the beads appear round, while being elliptical on the lower and upper plane. The ellipse major axis (x-axis or y-axis) depends on the molecule z-position compared to the focal plane for a particular image.

3. Image analysis

Calibration of the imaging system is a critical step before data analysis. Fluorescent beads immobilized on a coverglass are displaced in discrete steps along the optical axis. The beads appear in focus consecutively on the different panels of the image. The center positions of the different beads are then used to compute transformation matrices of the different panel images, compensating for any translation, rotation or magnification difference between the different imaging planes. This step allows computing the plane spacing at the specific imaging wavelength (as previously described in ref [3]).

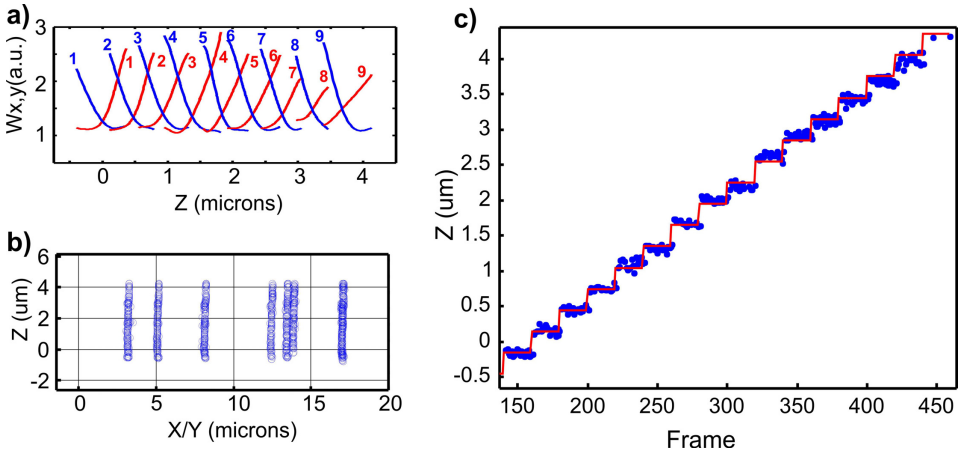

Fig. 2. a) Astigmatism calibration curves as recorded on each of the 9 subpanels spaced axially by 440 nm. The x (blue curve) and y (red curve) widths are plotted as an average of multiple acquisitions. b) localization of beads over the displacement range of 5 µm. c) computed axial position of fluorescent beads that are displaced by steps of 300 nm. At each step 20 time points are acquired to access localization precision.

In each image panel, the PSFs are fitted to a non-isotropic Gaussian profile, based on a modified version of Multi-Target Tracking (MTT) algorithm [8]. The ratio between the widths of the PSF minor and major axes are retrieved and averaged over many beads. The profile as a function of z position is fitted with a polynomial of 3rd degree. A look-up table is subsequently created containing the panel number and the polynomial factors. The widths of the ellipse along its main axes are shown in Fig. 2(a) as function of the bead position for all of the nine planes.

Each multifocal image goes through the following analysis steps. First, the transformation matrices are applied on the different sub panels of an acquired image. Contrary to our

#256814 Received 8 Jan 2016; revised 27 Jan 2016; accepted 27 Jan 2016; published 2 Feb 2016

previously reported application, the intensity (diffraction efficiency) difference between imaging planes is not accounted for. This difference is due mainly to imaging at a wavelength different from the one for which the grating was designed. In fact, in the current application, emitter position is defined to a single plane. Second, local maxima are fitted on each of the subpanels to an anisotropic 2D Gaussian function. The ratio between the widths of the two main axes is fed to the polynomial function specific to this plane in the lookup table. Thereby, the z position is computed relative to the imaged plane. Adding the plane axial position allows for the absolute real z-position to be determined. Third, the obtained positions are combined to a single localization file: detections appearing on consecutive planes are combined and averaged (Fig. 2(b)). When plane spacing is less than the depth of focus, molecules are expected to appear on two consecutive planes. If the localization appears on a single plane, then it is discarded as it is likely to be a false positive. This notably increases the quality and fidelity of the localizations. As an exception rule, localizations around the first and last planes are preserved without correlating them with adjacent planes. All computational and image analysis tools are custom-written in MATLAB.

To verify the robustness of this technique, we imaged beads immobilized on a coverglass using the astigmatic MFM and displaced the beads with discrete axial steps separated by 300 nm. A specific grating with 440 nm spacing was used in this experiment. At each step, 20 images are acquired and the axial positions retrieved as explained previously. In Fig. 2(c), we plot the axial positions as recorded by the MATLAB code. The axial localization accuracy was found to be 50 nm for a detected signal of 5000 photons per exposure, comparable to bright fluorophores signals.

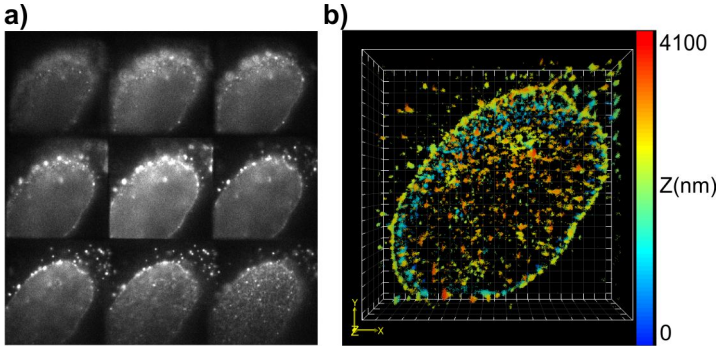

Fig. 3. Super-resolution imaging of the nucleopore complex with MFM and astigmatism with a plane spacing of 440 nm. a) MFM widefield image of the corresponding structure, b) the STORM reconstructed structure after 30000 frames acquisition of single molecule blinking. Molecules are localized on top and bottom of the nucleus.

4. Applications

To validate our ability to image single molecules in 3D, we performed super-resolution imaging of the nucleopore complex of a U2OS cell. Cells were transfected to express GFP attached to a nucleopore protein (NUP98) (Fig. 3(a)). After 24 hours, the cells were fixed with paraformaldehyde (PFA) for 15 minutes, and washed with PBS. After permeabilization and labeling with Alexa-647 tagged antiGFP-nanobodies, an imaging buffer was added for imaging in STORM mode. Fluorescent beads fixed on the coverglass served as fiducial markers for drift correction. Fluorescence images of single blinking molecules were recorded with 30 ms exposure time for approximately 15 minutes. Individual molecules were then localized and analyzed as previously described. As shown in Fig. 3(b), the full volumetric extent of the cell nucleus is recorded over 4.5 um axial range when imaged using a 440nm spacing between planes. In this example the plane spacing was below the depth of focus of the microscope objective that we used, meaning that localizations not appearing on several planes were discarded except for the first and last planes.

#256814 Received 8 Jan 2016; revised 27 Jan 2016; accepted 27 Jan 2016; published 2 Feb 2016

When imaging bright emitters, the signal to noise ratio is sufficient to alleviate the restriction on the plane spacing. To demonstrate this fact, we used 100 nm-radius fluorescent beads in a viscous fluid (glycerol:water 1:1 in volume), and imaged them using a grating of dz = 800nm spacing with the astigmatic lens. In this configuration, plane spacing is of the order of magnitude of the microscope objective depth of field. We then imaged the beads with 20 ms exposure time (Fig. 4(a), 4(b)), allowing us to recover trajectories over 7.2 µm depth (Fig. 4(c)). We analyzed the 3D trajectories of the particles by evaluating the mean square displacement (MSD) (Fig. 4(d)) and fitting it to the directed movement equation $MSD(T) = 6DT + (VT)^2 + b$, where D is the diffusion coefficient, T the time lag, V the particle velocity and b a constant. The distribution of diffusion coefficients peaked around 0.28 µm^2/s (Fig. 4(e)), in accordance with 0.27 µm^2/s the value expected from the Stokes–Einstein relation $D = K_B T / 6\pi\eta r$ for r = 100nm, and the viscosity η = 0.008 Ns/m^2 at 21°C of the glycerol/water mixture [9]. We could also retrieve the 3D flow velocity in our experiments, on the order of 5 µm/s, which is likely due to a combination of convection and spreading of the viscous fluid on the coverslip (Fig. 4(f)).

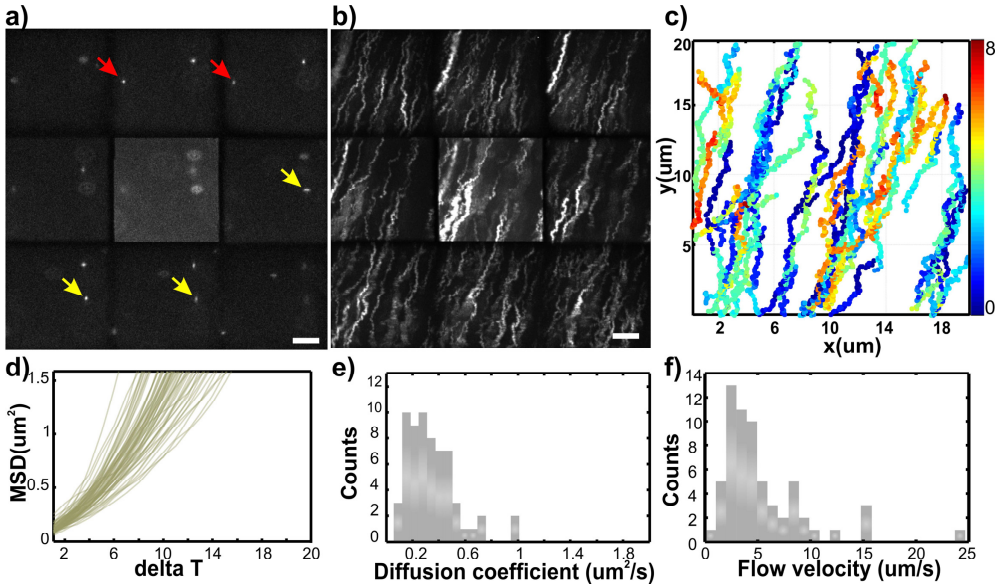

Fig. 4. Beads of 200 nm diameter are placed in a viscous fluid (1:1 mixture of water and glycerol). The beads are tracked in time while diffusing in a flow. The imaging was performed for a plane spacing of 800nm between planes. a) Snap shot in time of the fluorescent beads that can appear on multiple consecutive planes. However useful localization information is usually retrieved from one or two planes at most b) the maximum intensity snap shot of the acquired time frames showing the particles trajectories, c) localizations as computed by the MFM + astigmatism setup, d) the mean square displacement of the recorded trajectories e) 3D diffusion coefficient histogram showing a peak value around 0.28 µm^2/s, f) the flow velocity histogram.

5. Discussion and conclusion

We have shown in this paper that combining multifocus microscopy imaging with PSF engineering provides a useful tool for 3D single-particle imaging. In this configuration we report precise localization of single emitters over a 4.5 µm depth. Additionally, emissions localized on different image panels are compared to each other, allowing us to assert false positive detections. Combining the assigned molecules increases the localization precision in all directions. In this configuration the full volumetric imaging potential of the MFM is attainable, especially at detection volume edges. When spacing between planes is on the order of magnitude of depth of focus, only small axial overlap between planes is observed. In this

#256814 Received 8 Jan 2016; revised 27 Jan 2016; accepted 27 Jan 2016; published 2 Feb 2016

case, the full axial depth of the volumetric image ranges up to 8 μm, although bright emitters are required to achieve sufficient signal to noise ratios for single-particle localization.

The introduction of additional optical elements in the imaging system induces additional photon losses. Astigmatism further spreads the PSF photons over an extended elliptical shape. However, the precision and robustness of the current localization method can be improved by further increasing the number of collected photons. For instance, multiphase gratings can increase the photon collection by 30% [10]. Optical elements such as deformable mirrors for adaptive optics can also play a doubly beneficial role in improving the signal to noise ratio by: (i) collecting more photons and correcting optical aberrations when going deeper in a thick sample, and (ii) applying the astigmatic distortion without the introduction of an additional cylindrical lens [7]. Another approach consists in combining PSF engineering with multifocus gratings designed for diffraction for a smaller number of diffractive orders. Thereby, photons are split between fewer planes leading to better localization accuracy. Finally, it should be noted that different PSF engineering methods can be envisaged, such as the double helix PSF or Airy beams [11, 12], which show remarkable advantages when extended axial depth is desired. Combining multifocus microscopy with such methods would allow for deeper volumetric imaging for single-molecule localization and tracking.

Acknowledgments

B.H. acknowledges the financial support of the Pierre Gilles de Gennes Foundation, and Agence pour la Recherche sur le Cancer (ARC Foundation). We acknowledge financial support from French National Research Agency (ANR) Paris-Science-Lettres Program (ANR-10-IDEX-0001-02 PSL), France-Bio-Imaging infrastructure supported by ANR Grant ANR-10-INSB-04 (Investments for the Future) and the Institut Curie International PhD Program.

#256814 Received 8 Jan 2016; revised 27 Jan 2016; accepted 27 Jan 2016; published 2 Feb 2016